


ORIGINAL RESEARCH

Open Access



Evaluation of [^{13}N]ammonia positron emission tomography as a potential method for quantifying glutamine synthetase activity in the human brain

Alice Egerton^{1*†} , Joel T. Dunn^{2,3†}, Nisha Singh^{2,3,4,5}, Zilin Yu², Jim O'Doherty^{2,3,6}, Ivan Koychev^{1,5}, Jessica Webb², Simon Claridge², Federico E. Turkheimer⁴, Paul K. Marsden^{2,3}, Alexander Hammers^{2,3} and Antony Gee^{2,3}

Abstract

Purpose: The conversion of synaptic glutamate to glutamine in astrocytes by glutamine synthetase (GS) is critical to maintaining healthy brain activity and may be disrupted in several brain disorders. As the GS catalysed conversion of glutamate to glutamine requires ammonia, we evaluated whether [^{13}N]ammonia positron emission tomography (PET) could reliably quantify GS activity in humans.

Methods: In this test–retest study, eight healthy volunteers each received two dynamic [^{13}N]ammonia PET scans on the morning and afternoon of the same day. Each [^{13}N]ammonia scan was preceded by a [^{15}O]water PET scan to account for effects of cerebral blood flow (CBF).

Results: Concentrations of radioactive metabolites in arterial blood were available for both sessions in five of the eight subjects. Our results demonstrated that kinetic modelling was unable to reliably distinguish estimates of the kinetic rate constant k_3 (related to GS activity) from K_1 (related to [^{13}N]ammonia brain uptake), and indicated a non-negligible back-flux of [^{13}N] to blood (k_2). Model selection favoured a reversible one-tissue compartmental model, and [^{13}N]ammonia K_1 correlated reliably ($r^2 = 0.72\text{--}0.92$) with [^{15}O]water CBF.

Conclusion: The [^{13}N]ammonia PET method was unable to reliably estimate GS activity in the human brain but may provide an alternative index of CBF.

Keywords: Glutamate, Glutamate turnover, PET, Test–retest, Arterial input function, Metabolites, CBF, Cerebral blood flow, One-tissue compartment model

Introduction

The metabolism of glutamate to glutamine by the enzyme glutamine synthetase (GS) is a key process for maintaining healthy synaptic function. GS (encoded by

the gene glutamate-ammonia ligase, *Glul*) is predominantly expressed in astrocytes [1] and converts glutamate released into the synapse during neurotransmission to glutamine, for recycling to neuronal glutamate and gamma-amino butyric acid (GABA). GS is therefore critical to the homeostasis of excitatory and inhibitory neurotransmission and normal brain activity [2, 3]. This process may be compromised in several brain disorders [3], and neuroimaging techniques to assess GS

*Correspondence: Alice.Egerton@kcl.ac.uk

†Alice Egerton and Joel T. Dunn: Joint first authorship

¹ Department of Psychosis Studies, Institute of Psychiatry, Psychology and Neuroscience, King's College London, 16 De Crespigny Park, London SE5 8AF, UK

Full list of author information is available at the end of the article

activity in vivo could have wide-ranging research or clinical impact.

Abnormalities in GS have been most clearly linked to epileptogenesis [4]. Very rare inherited deficits in GS are associated with neonatal seizures [5, 6]. Pharmacological inhibition of GS [2] or genetic GS deficiency [7] can be used as animal models of epilepsy, and there are marked reductions in GS in areas of hippocampal tissue resected from patients with mesial temporal lobe epilepsy [8, 9]. Furthermore, regional differences in the level of GS protein, mRNA expression or activity have been detected in post-mortem brain tissue across many psychiatric and neurological disorders. The results of these studies, summarised in Additional file 1: Table S1, suggest that in addition to applications in epilepsy, GS imaging could be important in understanding or predicting schizophrenia, depression or suicidal behaviour, amongst other disorders.

GS is also the main pathway for metabolism of brain ammonia, which is required for the conversion of glutamate of glutamine [10]. This raises the possibility that radiolabelled ammonia in combination with positron emission tomography (PET) may be utilised to measure brain GS activity. [¹³N]Ammonia PET is used clinically to assess myocardial perfusion (“blood flow”) and has been applied in research studies examining abnormalities in brain ammonia uptake associated with liver disease [11–20] and in the diagnosis of brain tumours [21].

The aim of this study was to evaluate [¹³N]ammonia as a PET tracer for quantification of brain GS activity. This evaluation requires kinetic modelling of the dynamic concentrations of ¹³N-derived radioactivity in the brain and arterial blood following radiotracer injection, in an attempt to reliably extract rate constants, as the rate of conversion of [¹³N]ammonia to [¹³N]glutamine, from the signal relating to [¹³N]ammonia brain uptake and clearance (see Additional file 1: Figure S1). To do this we sought to acquire two [¹³N]ammonia scans (test and re-test) in eight healthy volunteers. In order to account for effects of cerebral blood flow (CBF), we additionally acquired test and re-test [¹⁵O]water PET scans in the same subjects on the same day, with [¹⁵O]water PET scans preceding [¹³N]ammonia PET.

Primary analysis of the suitability of the method assessed the identifiability and repeatability of the k_3 rate-constant representing GS activity in the kinetic model (see Additional file 1: Figure S1). While this is not sufficient to prove evaluation of GS activity, it would be a pre-requisite to using this standard kinetic modelling approach. Secondary analysis assessed identifiability and repeatability of other parameters, kinetic model selection, and comparisons to previous work using [¹³N]ammonia to evaluate blood–brain-barrier function [11].

Methods

The study had ethical approval from the NHS Ethical Committee (NRES South East Coast, Surrey), the local Research and Development offices and the Administration of Radioactive Substances Advisory Committee (ARSAC). Participation required provision of written informed consent to all study procedures.

Participants

The study aimed to acquire complete datasets (including one T1-weighted MRI scan, two [¹³N]ammonia scans and two [¹⁵O]water PET scans) in eight healthy volunteers. Participants were recruited internally through King’s College London’s recruitment system. Inclusion required that participants were aged 18 or older and were able to provide written informed consent in English. Exclusion criteria included the standard contraindications to PET and MRI, including pregnancy. Absence of pregnancy in female participants was confirmed by a negative urine pregnancy test on arrival to the PET scanning visit.

MRI

MRI scans were performed at the Centre for Neuroimaging Sciences, King’s College London, UK on a General Electric MR750 3T MRI scanner. A T1-weighted structural MRI scan based on the ADNI protocol (voxel size $1.05 \times 1.05 \times 1.20$ mm, TE 3.016 ms; TR 7.312 ms matrix 256×256 ; FoV 270 mm; inversion time 400 ms) was acquired for co-registration of the participants’ PET images.

Radiochemistry

Aqueous [¹³N]ammonia was produced on a CTI RDS 112 biomedical cyclotron via the ¹⁶O(p,α)¹³N nuclear reaction. The target contained 8 mL H₂O with 5 mM ethanol according to Wieland et al. [22].

[¹⁵O]water: Oxygen-15 was produced in the form of [¹⁵O]oxygen gas by the bombardment of enriched [¹⁵N]nitrogen gas containing 1–2.5% oxygen gas via the ¹⁵N(p,n)¹⁶O nuclear reaction. [¹⁵O]water was subsequently obtained by passage with hydrogen over a platinum catalyst according to Berridge et al. [23].

PET image acquisition

PET scans were acquired at St Thomas’ Hospital, King’s College London on a GE Discovery 710 PET-CT scanner with 3D acquisition and list mode. Each participant underwent two PET scanning sessions, performed in the morning and afternoon of the same day. Each of the two scanning sessions consisted of an initial low dose CT scan to enable correction for tissue attenuation of radioactivity, a dynamic [¹⁵O]water scan (5 min), and a dynamic [¹³N]ammonia scan (30 min).

There was a break of approximately one hour between the two sessions, during which lunch was provided, and an appropriate gap (at least 5 half-lives) between subsequent scans to avoid residual counts (i.e. at least 10 min following the [^{15}O]water scans and 50 min following the [^{13}N]ammonia scan).

At the start of the PET scan visit, a cannula was inserted in a vein in the arm for radiotracer injection. After application of local anaesthetic, an arterial line was inserted into the radial artery and flushed every 20 min with heparinised saline (20 IU/mL of heparin in sterile 0.9% w/v sodium chloride) until removal at the end of PET scanning. Just before the start of each scanning session, 6 mL of arterial blood was taken to measure baseline blood ammonia levels.

Participants were positioned in the PET-CT scanner, with head movement minimised via a moulded headrest and head strap. The arterial cannula was connected to an automated blood sampling system (Allogg ABSS, www.allogg.se, Sweden) using a 150 cm PTFE coated tubing (inner diameter 1 mm). CT scout (0.015 mSv) and CT attenuation correction (0.05 mSv) scans were acquired. ^{15}O -water (target dose at time of administration: 960 MBq, 1.10 mSv) was injected through the venous cannula over 10 s. PET image acquisition started 10 s before the start of [^{15}O]water injection and continued for a total of 5 min. Arterial blood collection via the fluid analyser commenced 70 s before [^{15}O]water injection and 60 s before the start of scan acquisition and continued for the 5 min scan duration, to a total of 25 mL. Additionally, a single 2 mL arterial blood sample was manually drawn at 4 min into the scan.

After completion of the [^{15}O]water scan the arterial line was flushed with heparinised saline. At least 20 min after the end of the ^{15}O -water scan (25 min after [^{15}O]water injection), [^{13}N]ammonia (target dose at time of administration: 550 MBq, 1.5 mSv) was injected through the venous cannula. PET image acquisition started 10 s before the start of [^{13}N]ammonia injection and continued for 30 min. Arterial blood collection via the fluid analyser commenced 70 s before [^{13}N]ammonia injection and 60 s before the start of scan acquisition and continued for 15 min, to a total of 75 mL. In addition, 6 manual arterial blood samples of 10 mL each were drawn at 4, 6, 8, 12, 20 and 30 min after scan start during the [^{13}N]ammonia scans, which were used for whole blood, plasma and metabolite analysis.

In the second session, a minimum of 1 h later, both the [^{15}O]water and [^{13}N]ammonia scans were repeated using identical acquisition protocols.

Ammonia and metabolite analysis

The method used for separation of ammonia and metabolite from plasma samples was based on the method published by Keiding et al. [11] and is described below.

Levels of non-radioactive ammonia in arterial blood were determined from samples collected before radiotracer collection. These samples were collected in K-EDTA tubes (pre-tested and confirmed as ammonia-free) and transported on ice within 20 min of collection to the hospital laboratory for standard analysis.

Unless stated otherwise, all water used in these metabolite analyses was passed through ion exchange resin and 0.22 μm membrane filtered to produce water with a specific resistance of 18.2 micro-ohms using a Milli-Q Ultrapure water purification system manufactured by Millipore Corporation.

Plasma was separated from whole blood by centrifuging at $3000 \times g$ for 3 min at room temperature (RT). Levels of radioactive metabolites in plasma were estimated through solid phase extraction, based on the methods of Keiding et al. [17]. In preparation for solid phase extraction, one cartridge was filled with 0.6 mL Dowex 1X8-50 anion exchange resin and pre-treated with 6 mL 0.75 M sodium acetate solution. A second cartridge, connected in series via an Agilent Bond Elut adapter, was filled with 0.35 mL AG50W-X8 cation exchange resin and pretreated with 3.5 mL 0.8 M Tris-acetate solution. The third cartridge which connected to the second cartridge in the same way via adapter was filled with 0.35 mL AG50W-X8 cation exchange resin and pretreated with 3.5 mL Millipore water.

For extraction, 0.5 mL of the supernatant protein-free plasma was loaded onto the first cartridge followed by washing with 3 mL of Millipore water through the cartridge stack and flushed with 10 mL of air. The eluent from the first cartridge passed through the second cartridge and third cartridge, which were subsequently washed with 7 mL of Millipore water followed by 10 mL of air. The third cartridge was washed with 7 mL Millipore water and followed by 10 mL of air. All eluates were collected with a 25 mL pot. With this method, the radioactivity measured on the first cartridge corresponded to [^{13}N]glutamate, on the second cartridge corresponded to intact [^{13}N]ammonia, on the third cartridge corresponded to [^{13}N]glutamine, and the pot corresponded to [^{13}N]urea.

A 10-detector gamma-counter (Wizard2 2470, Perkin-Elmer) cross-calibrated to the PET scanner was used to measure radioactivity concentrations in whole blood (0.5 mL per sample), plasma (0.5 mL per sample) and metabolite fractions (3 mL for urea and full cartridge contents for other fractions). All samples were counted for 3 min on a fixed energy window (358–664 keV) with

software cross-talk correction and in-house volumetric geometry correction. The samples and cartridges were corrected for weight to calculate the total radioactivity of blood sample analysed. All sample data were background and decay corrected to scan start time prior to data analysis.

Image processing

[¹⁵O]water PET list mode data was unlisted to 26 frames (1×10 s, 10×5 s, 6×10 s and 9×20 s). [¹³N]ammonia PET list mode was unlisted to 47 frames (1×10 s, 10×5 s, 6×10 s, 3×20 s, 27×60 s). All PET images were reconstructed to a 256^2 matrix with 47 slices with $0.98 \times 0.98 \times 3.27$ mm voxel size, 3D iterative reconstruction (GE “VuePoint”, 4 iterations, 24 subsets, 4 mm FWHM Gaussian post-filter), scatter correction and inter- and intra-frame decay correction. Images were reconstructed with CT attenuation correction (attenuation corrected, AC) and without (non-attenuation corrected, NAC).

Frame-by-frame motion correction was performed on dynamic PET data using the NAC image to derive the rigid-body motion parameters which were applied to the paired AC image (first 9 frames ignored to avoid low counts). Regions of interest (ROI) were defined by the “Hammers_mith Atlas” [24, 25] (83 regions) in MNI stereotaxic space. Nonlinear warps from MNI to subject space were defined using the unified segmentation algorithm [26] in SPM8 (www.fil.ucl.ac.uk/spm) on each subject’s T1 MRI. Resliced atlases for each subject were then co-registered to a summed PET image (sum of total scan duration of motion corrected AC image ignoring first 60 s) for each PET scan via the MRI.

For both the [¹⁵O]water and [¹³N]ammonia scans, time activity curves (TACs) were extracted from the co-registered Hammers_mith atlas [24, 25] (ignoring ventricular and white matter regions). Using each subject’s co-registered probabilistic grey matter mask from the segmented MRI, TACs were extracted using the mean voxel value within the region or a weighted mean for cortical regions using each subject’s grey matter probabilistic mask. Whole-brain grey matter and white matter weighted mean TACs were also defined. A total of 79 regions were explored (77 atlas ROIs plus global grey and white matter).

Blood data processing

For the [¹³N]ammonia scans, arterial whole blood input functions were created from decay-corrected continuous blood samples with manual samples used for cross-calibration to scanner and interpolation to scan end. Plasma-over-blood ratio was calculated as the mean of the manual plasma and whole blood sample ratios for each

subject (Additional file 1: Figure S2). Parent fraction data (ratio of [¹³N]ammonia to total ¹³N activity) was fitted to a biexponential curve for each subject as used by Keiding et al. [11]. Parent plasma input functions (i.e. [¹³N]ammonia in plasma only) for the kinetic modelling were created by multiplying the whole-blood input function by plasma-over-blood ratios and the biexponential curve fitted to the parent fractions. To account for delay between the blood sampling detector and PET scan whole blood and parent plasma input functions were delay corrected by visually matching the blood rise with the grey matter TAC, with decay correction.

Kinetic analysis

Regional cerebral blood flow (CBF) was calculated from the [¹⁵O]water TACs using the 5-parameter free diffusion model as described by Meyer [27] applied to each time activity curve. In brief, a nonlinear least squares fit method was used to simultaneously estimate the 5 free parameters of this 1-tissue compartment model: CBF, $k_{1/2}$ (¹⁵O wash-out), blood fraction, and delay and dispersion of the blood curve between the brain and sampling point (in addition to the visual delay correction described above).

Ammonia is a freely diffusible tracer and as such has been used to quantify perfusion in myocardium [28] and brain [29]. Though ammonia is rapidly trapped in tissue, in order to index GS activity, the kinetic parameters describing the uptake of [¹³N]ammonia by GS must be distinguishable from those reflecting CBF. The model chosen for primary analysis of [¹³N]ammonia scans was an irreversible two tissue compartment model (2TCM) as used in Keiding et al. [11]. To confirm the model choice a nonlinear spectral analysis approach was used to identify the most appropriate tissue uptake model [30]. In brief, the data was fitted to a number of candidate PET compartmental models with increasing numbers of parameters. In this case, a reversible 2TCM [Additional file 1: Figure S1] was the most complex model considered, with increasingly simpler models defined by setting k_4 , k_3 , k_2 to zero (i.e. 4 candidate models). The blood fraction contributing to the TAC for each region was also included as a free parameter.

Each compartmental model was fitted using a weighted least squares method with weighting inversely proportional to the variance of each frame determined by frame duration and radioactive decay: $\Delta_i e^{-\lambda t_i}$, where λ is the decay rate constant, and Δ_i and t_i are the frame duration and frame mid-point time, respectively, for frame i .

Additional macroparameters from the ¹⁵O and ¹³N scans were calculated to compare with the results of Keiding et al. [11]. These parameters are not directly of interest to the identification of the k_3 parameter, but were

obtained solely for the purpose of comparison. PS_{BBB} (flow independent permeability-surface area product of the blood brain barrier to $[^{13}N]$ ammonia) was calculated as

$$PS_{BBB} = -CBF \ln(1 - K_1/CBF)$$

where CBF is calculated from the $[^{15}O]$ water scan (assuming a 100% extraction fraction), and K_1 from the $[^{13}N]$ ammonia scan. Extraction Fraction (EF) was also calculated as the simple ratio of K_1 to CBF. Net metabolic clearance of $[^{13}N]$ ammonia in blood into intracellular $[^{13}N]$ glutamine, K_{met} , was calculated using the Patlak graphical method using the complete data, with a t^* of 20 min [32]. PS_{met} (flow-independent permeability-surface area product of conversion of ammonia to intracellular glutamine) was calculated as

$$PS_{met} = -CBF \ln(1 - K_{met}/CBF)$$

Finally, metabolic flux of ammonia molecules from blood to glutamine in tissue, $Flux_{met}$, (as described by Keiding et al. [11]), was calculated as

$$Flux_{met} = K_{met}A$$

where A is the measured concentration of endogenous ammonia in the blood.

Statistical analysis

Identifiability of the k_3 rate-constant from the $[^{13}N]$ ammonia data was evaluated by testing if the estimated parameter value, relative to estimated error, was significantly greater than zero (using the one-sided t -test). For the irreversible 2TCM model (4 parameters) with 47 frames, this corresponds to a proportional estimate parameter error of 39%. In addition, optimal model selection on the $[^{13}N]$ ammonia data was assessed using the Akaike Information Criterion (AIC) [31].

Kinetic parameter repeatability between the test-retest scans was assessed using mean fractional difference (VAR), absolute fractional difference (AbsVAR), and intraclass correlation coefficient (ICC) using a two-way random model for consistency [33]. For 8 subjects, the threshold for a significantly positive ICC is 0.58 at the $p < 0.05$ level. VAR and AbsVAR were calculated for N subjects as a percentage:

$$VAR = \frac{1}{N} \sum_{i=1}^N 200 \times \frac{\text{retestValue}_i - \text{testValue}_i}{\text{testValue}_i + \text{retestValue}_i}$$

$$AbsVAR = \frac{1}{N} \sum_{i=1}^N 200 \times \frac{|\text{testValue}_i - \text{retestValue}_i|}{\text{testValue}_i + \text{retestValue}_i}$$

Image registration, TAC extraction, blood data processing, kinetic modeling and statistical analyses were performed in MATLAB (www.mathworks.com). Data are presented as mean \pm s.d. unless otherwise stated.

Results

Participants

Eight volunteers (3 female) underwent all PET-CT and MRI scans. Age at scan was 25.0 ± 2.5 years. Weight, height and BMI were 75.7 ± 9.3 kg, 1.74 ± 0.13 m and 25.3 ± 4.1 kg/m², respectively.

Scan parameters

Ammonia blood levels immediately prior to scan session one were 24.5 ± 5.7 $\mu\text{mol/L}$ and prior to session two 23.9 ± 4.8 $\mu\text{mol/L}$. No significant difference was found between scan session within-subject (0.6 ± 7.9 $\mu\text{mol/L}$; range -12.0 to 11.0). No significant differences were observed for the administered $[^{15}O]$ water (mean \pm s.d. = 841 ± 126 MBq, and 834 ± 146 MBq for sessions one and two, respectively) or the $[^{13}N]$ ammonia (mean \pm s.d. = 537 ± 7 MBq and 537 ± 3 MBq for sessions one and two, respectively). Additionally, no significant differences were observed between the timings between sessions one and two. The mean time between $[^{15}O]$ water and $[^{13}N]$ ammonia injections was 48 ± 6 min and 46 ± 4 min for sessions one and two, respectively, with a minimum gap of 37 min. The mean time between first $[^{13}N]$ ammonia and second $[^{15}O]$ water injections was 88 ± 33 min (minimum 65 min).

$[^{15}O]$ water: kinetic analysis and repeatability

Visual inspection indicated that grey matter TAC fits were excellent (Additional file 1: Figure S2). Grey matter CBF was 37.6 ± 4.8 and 38.5 ± 3.4 mL/100 g/min for sessions one and two, respectively (Table 1, no significant difference). Repeatability of CBF calculations across 8 subjects was moderate (Table 2) and ICC values were significantly > 0 in 44 of 77 individual grey matter ROIs (mean ICC = 0.58 ± 0.23) and the white matter, but not in the whole brain grey matter TACs (ICC = 0.50). VAR and AbsVAR were 2.7% and 8.6%, respectively, for grey matter. Across individual ROIs, the mean \pm s.d. values for VAR and AbsVAR were $2.3 \pm 2.5\%$ and $9.7 \pm 2.5\%$, with values below 10% in 50 of 77 ROIs. Statistics for all parameters in this model are shown in Additional file 1: Tables S4 and S5 with TACs and fits in Additional file 1: Figure S6.

$[^{13}N]$ ammonia: metabolite analysis

Continuous and manual blood sampling was obtained for all scans in all 8 subjects. $[^{13}N]$ ammonia and $[^{13}N]$ metabolite fractions were successfully obtained for the

Table 1 Model parameters for test (S1) and retest (S2) scans for grey matter and selected regions of interest (ROIs)

ROI	¹⁵ O]water [<i>n</i> = 8]		¹³ N]ammonia [<i>n</i> = 5]					
	CBF (mL/100 g/min)		<i>K</i> ₁ (mL/100 g/min)		<i>k</i> ₂ (1/min)		<i>k</i> ₃ (1/min)	
	S1	S2	S1	S2	S1	S2	S1	S2
Grey Matter	37.6 ± 4.8	38.5 ± 3.4	20.1 ± 1.5	18.7 ± 1.3	0.0072 ± 0.0035	0.0096 ± 0.0042	0.0031 ± 0.0045	0.0177 ± 0.0259
White Matter	25.8 ± 3.4	26.4 ± 2.7	14.6 ± 1.1	13.7 ± 0.7	0.0073 ± 0.0043	0.0096 ± 0.0053	0.0139 ± 0.0177	0.0274 ± 0.0401
Hippocampus_l	32.1 ± 3.7	33.8 ± 3.1	19.7 ± 2.8	18.8 ± 1.6	0.0256 ± 0.0145	0.0360 ± 0.0212	0.0532 ± 0.0261	0.0621 ± 0.0304
OL_ling_G_l	40.8 ± 5.4	41.5 ± 2.8	23.7 ± 3.0	21.6 ± 0.9	0.0072 ± 0.0023	0.0090 ± 0.0035	0.0000 ± 0.0000	0.0125 ± 0.0172
G_cing_post_l	43.6 ± 5.3	44.3 ± 4.2	22.2 ± 1.6	20.8 ± 1.3	0.0069 ± 0.0038	0.0099 ± 0.0059	0.0038 ± 0.0052	0.0154 ± 0.0231
Putamen_l	45.3 ± 7.3	46.1 ± 5.5	23.3 ± 1.9	21.2 ± 1.5	0.0063 ± 0.0028	0.0086 ± 0.0037	0.0000 ± 0.0000	0.0144 ± 0.0203
Thalamus_l	43.9 ± 5.5	44.5 ± 4.2	22.8 ± 2.4	21.2 ± 1.2	0.0128 ± 0.0057	0.0178 ± 0.0075	0.0241 ± 0.0214	0.0405 ± 0.0234
Cerebellum_l	41.7 ± 6.8	42.6 ± 5.2	22.5 ± 2.0	20.7 ± 1.3	0.0070 ± 0.0047	0.0088 ± 0.0034	0.0056 ± 0.0126	0.0145 ± 0.0216

The table presents estimates of cerebral blood flow (CBF) from [¹⁵O]water scans, and irreversible two tissue compartmental model parameter estimates for rate constants *K*₁, *k*₂ and *k*₃ from [¹³N]ammonia scans. Data are presented as mean ± standard deviation for grey matter, white matter and the left (l) hippocampus, lingual gyrus (OL_ling_G), posterior cingulate gyrus (G_cing_post), putamen, thalamus, and cerebellum

Table 2 Repeatability metrics for [¹⁵O]water cerebral blood flow (CBF) and [¹³N]ammonia two tissue compartment model parameters for grey matter and selected regions of interest (ROIs)

ROI	¹⁵ O]water [<i>n</i> = 8]			¹³ N]ammonia [<i>n</i> = 5]								
	CBF			<i>K</i> ₁			<i>k</i> ₂			<i>k</i> ₃		
	ICC	VAR	AbsVAR	ICC	VAR	AbsVAR	ICC	VAR	AbsVAR	ICC	VAR	AbsVAR
Grey Matter	0.50	3 ± 11	9 ± 6	-0.79	-7 ± 13	10 ± 11	0.94	29 ± 18	29 ± 18	0.02	-30 ± 179	153 ± 62
White Matter	0.69	2 ± 10	7 ± 6	-0.89	-6 ± 13	9 ± 10	0.93	28 ± 18	28 ± 18	-0.05	-46 ± 163	141 ± 67
Hippocampus_l	0.17	5 ± 13	11 ± 9	0.35	-4 ± 13	10 ± 8	0.62	34 ± 44	48 ± 23	0.22	15 ± 49	39 ± 27
OL_ling_G_l	0.22	2 ± 13	10 ± 9	-0.42	-8 ± 15	10 ± 14	0.86	21 ± 13	21 ± 13	-0.00	71 ± 165	147 ± 80
G_cing_post_l	0.68	2 ± 9	8 ± 4	-0.78	-7 ± 13	9 ± 11	0.86	34 ± 24	34 ± 24	0.15	13 ± 196	173 ± 37
Putamen_l	0.85	2 ± 8	7 ± 2	-0.84	-9 ± 14	12 ± 12	0.85	31 ± 24	31 ± 24	-0.00	59 ± 194	181 ± 33
Thalamus_l	0.66	2 ± 9	7 ± 5	-0.64	-7 ± 15	11 ± 11	0.76	35 ± 27	37 ± 25	0.42	80 ± 95	105 ± 57
Cerebellum_l	0.69	3 ± 12	9 ± 7	-0.58	-8 ± 13	9 ± 13	0.91	30 ± 27	32 ± 24	0.22	-58 ± 157	138 ± 73

The table presents the intraclass correlation coefficient (ICC), percent mean fractional difference (VAR) and percent absolute fractional difference (AbsVAR) across test and retest scans. Data are presented as mean ± standard deviation for grey matter, white matter and the left (l) hippocampus, lingual gyrus (OL_ling_G), posterior cingulate gyrus (G_cing_post), putamen, thalamus, and cerebellum

first five subjects but appeared as outliers in the subsequent three subjects (Fig. 1). The source of these outliers is unknown but potentially due to issues with later preparation of solid phase extraction materials. In the first 5 subjects, biexponential curve fits to parent fractions were in line with results from Keiding et al. [11]. Data from these 5 subjects were used to determine the [¹³N]ammonia kinetic model parameter fits and repeatability. Plasma over blood fractions are shown in Additional file 1: Figure S2. Fits were only performed to the parent fraction though individual ¹³N labelled compound fractions are shown in supplementary data (Additional file 1: Figure S3). For all subjects, input functions with grey matter TACs for comparison are shown in Additional file 1: Figures S7 and S8.

[¹³N]ammonia: *k*₃ identifiability and model selection

Across 5 subjects, 2 scans and 79 ROIs, 790 TACs were analysed using the irreversible 2TCM [11]. No region showed a nonzero *k*₃ value across all subjects and scans, indicating trapping of ¹³N was either inconsistent or negligible. Overall, only 54/790 TACs estimated significantly positive *k*₃ (*p* < 0.05), but this was not consistent across pairs of scans. For comparison, by the same criteria, *K*₁ was nonzero in 779/790 regions, and *k*₂ in 452/790 (Additional file 1: Table S12).

Using AIC to compare the results of alternative candidate kinetic model fits, no regions showed best fits to the irreversible 2TCM consistently across all subjects and scan pairs, again reflecting negligible trapping. Of 790 TACs, 656 fit the reversible 1TCM best, with 109

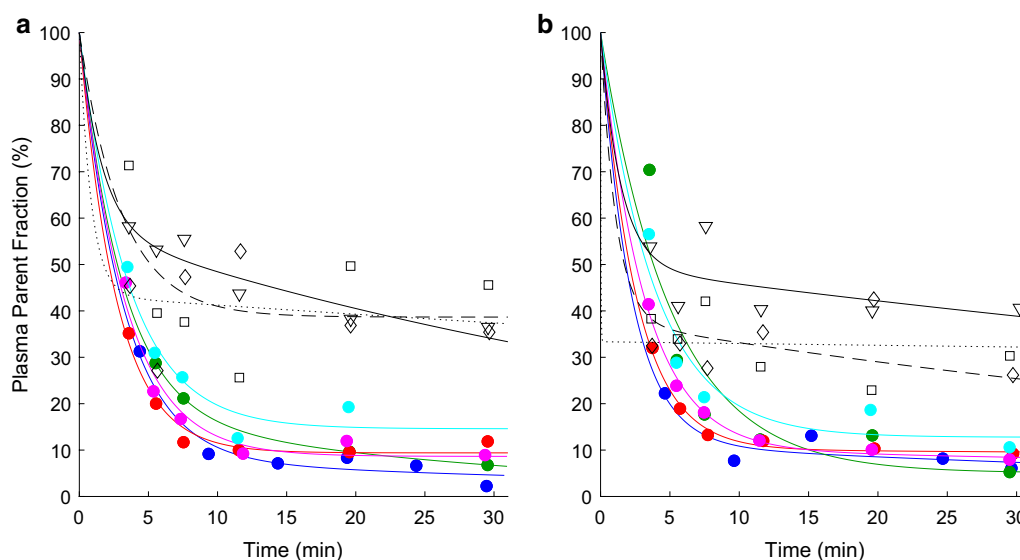


Fig. 1 Plasma parent fraction data and fit. Plasma parent fraction for **a** test scan and **b** retest scan for each subject. Symbols represent ratio of parent compound, [^{13}N]ammonia, to total ^{13}N labelled fractions (parent plus metabolites) measured from individual arterial plasma samples. Lines show biexponential fits to subject/scan data sets. Coloured lines and circles show colour-coded subjects 1–5 used in the full analysis (blue, green, red, magenta and cyan, for subjects 1–5, respectively). Black symbols and lines (triangle/solid, square/dashed, diamond/dotted for subjects 6–8, respectively) show subjects 6–8 considered corrupted data. X-axis is time in minutes from injection (corrected for brain-detector delay). Y-axis is plasma parent fraction in percent

preferring the standard irreversible 2TCM. Looking at consistency of model choice across scan pairs, 70 of 79 regions selected the reversible 1TCM across a majority of subjects. Only one region, left hippocampus, selected the irreversible 2TCM in a majority of subjects: 3/5 (this was also the case when including all 8 subjects: 5/8). Note, in this region, k_3 ICC and interscan variability was also poor (Table 1). The remaining models showed no consistent model preference across subjects and scans: 24/790 TACs preferred irreversible 1TCM and 1/790 preferred reversible 2TCM (Additional file 1: Table S13, with graphical representation across all subjects and regions in Additional file 1: Figure S4).

^{13}N]ammonia: kinetic analysis and repeatability

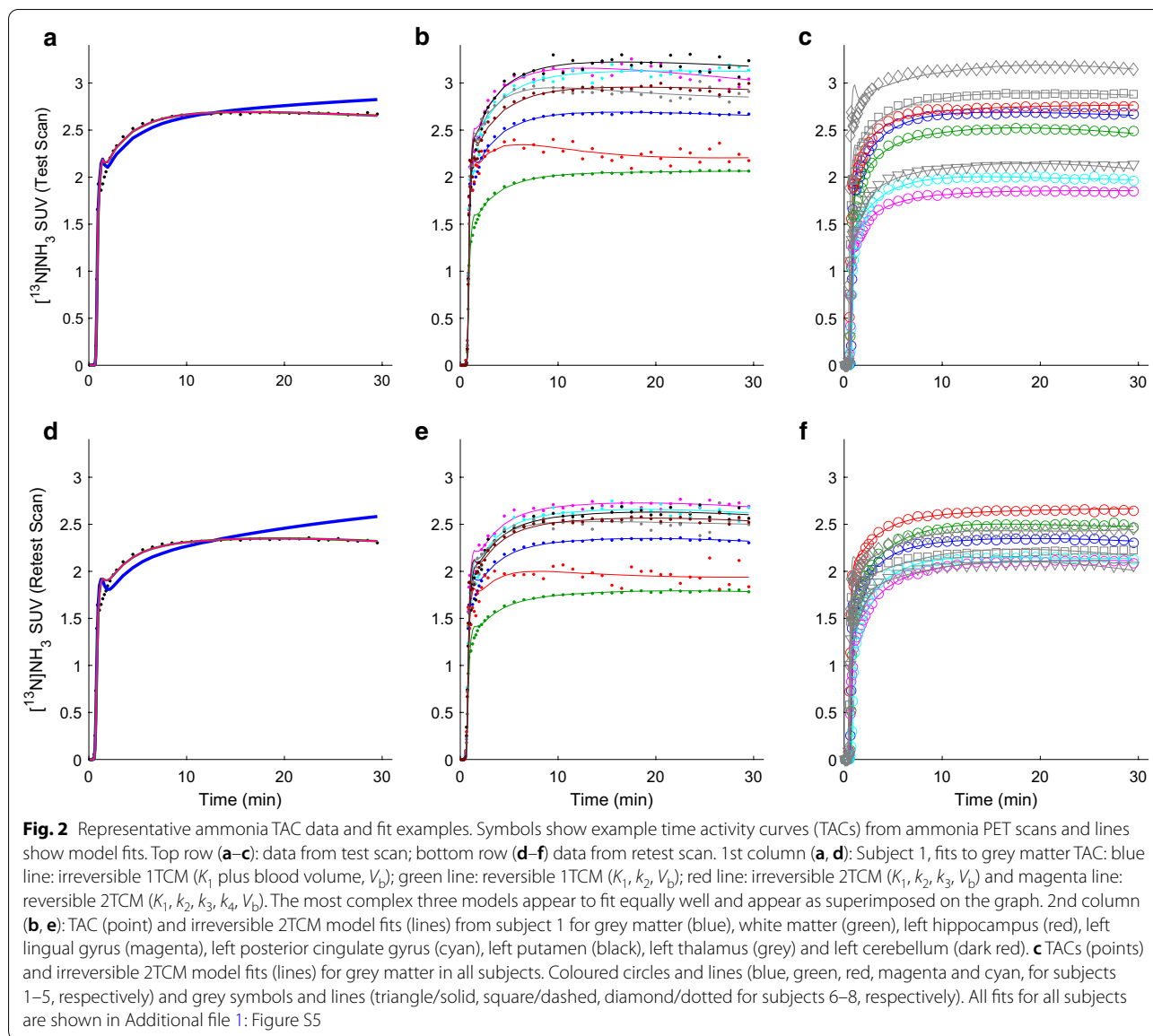
^{13}N]ammonia PET images showed regional variation in signal intensity, with highest uptake in the occipital lobes, posterior cingulate gyri, putamina, thalami and cerebella. Figure 2 shows example TACs and fits (further data in Additional file 1: Figure S5). Table 1 presents K_1 , k_2 and k_3 values for the [^{13}N]ammonia scans from subjects 1–5, calculated using the irreversible 2TCM across grey matter and in selected high uptake ROI in the left hemisphere (additional statistics in Additional file 1: Tables S6–S9). K_1 values were comparable between subjects and scan sessions. K_1 ICC values (Table 2) were negative indicating poor repeatability, though absolute fractional

differences were comparable to those of CBF, indicating the negative ICC values are a consequence of low inter-subject variability. Values for washout (k_2) and trapping (k_3) rate constants (Table 1) were small and highly variable across region, subject and scan. ICC values were high for k_2 despite large differences between the test and retest scans (Table 2). This is likely to be due to the even larger variation in k_2 values across subjects rather than reflecting strong test–retest repeatability. Test–retest variation in the trapping rate constant k_3 was extremely poor (Table 2).

The results from the majority-preferred reversible 1TCM are shown in Table 3 (further statistics in Additional file 1: Tables S10 and S11). The repeatability metrics for K_1 and k_2 calculated using the 1TCM (Table 3) were similar to those calculated using the 2TCM (Table 2). K_1 continued to show low or negative ICC values and fractional differences of approximately 10%; k_2 showed higher ICC but larger inter-subject variability and test–retest differences. Volume of Distribution (K_1/k_2) was also calculated but this too had high intra-subject variability.

Including data from all 8 subjects (Additional file 1: Tables S8 and S9) did not improve repeatability.

The values obtained for K_{met} , PS_{met} and Flux_{met} showed quite high fractional differences across test and retest scans (Additional file 1: Table S2). PS_{bb} and EF showed



lower intrasubject variability but also low ICC values (Additional file 1: Table S3).

Finally, the degree to which CBF may have accounted for brain uptake of $[^{13}\text{N}]$ ammonia was investigated by examining the correlations between $[^{15}\text{O}]$ water CBF and $[^{13}\text{N}]$ ammonia K_1 (as estimated through the irreversible 2TCM or reversible 1TCM) or K_{met} . Correlating within each scan pair (across all ROIs), K_1 estimates from 1TCM were most highly correlated with CBF in all 10 scan pairs, with r^2 values ranging from 0.72 to 0.92 (Fig. 3). In each of the 10 scan pairs, r^2 values were second highest with the 2TCM K_1 (r^2 between 0.56 and 0.85) and poorest and most variable with K_{met} (r^2 between 0.2 and 0.85). However, these strong within-subject correlations were

not replicated across subjects within region: no region revealed a significant positive correlation between CBF and K_1 or K_{met} .

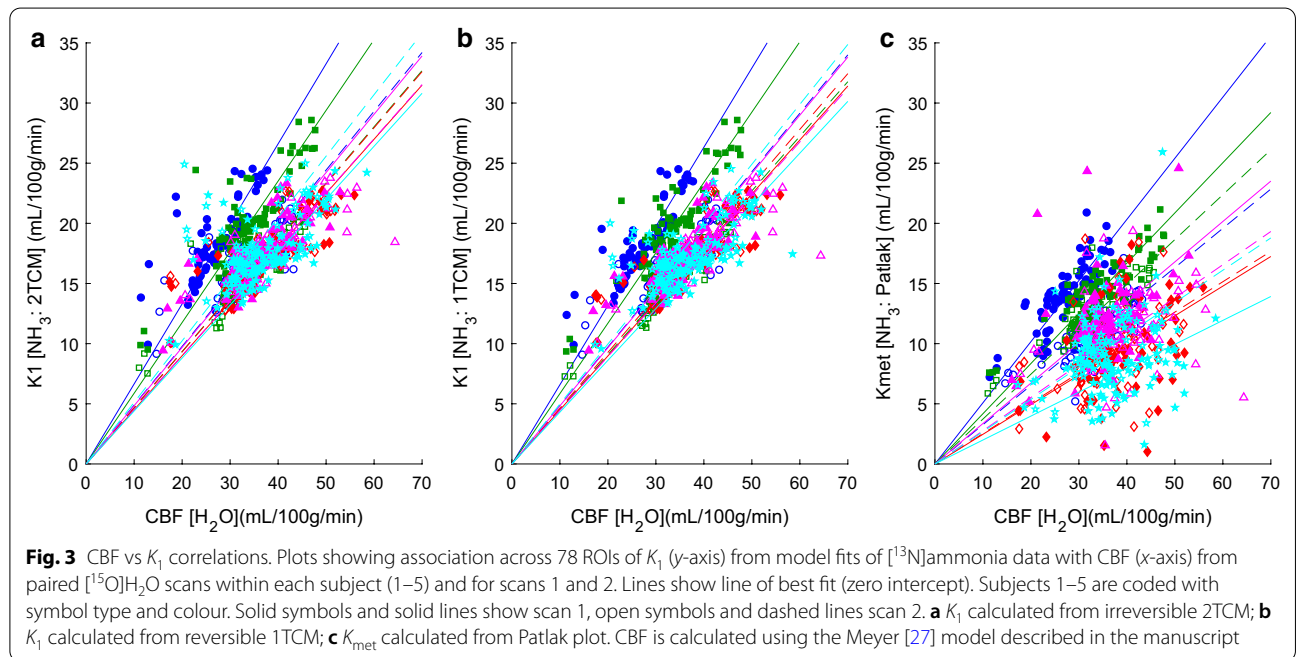
Discussion

This study evaluated kinetic models for $[^{13}\text{N}]$ ammonia PET as an in vivo method to assess whether a reliable estimate of trapping could be determined which could be a basis for estimating the rate of conversion of glutamate to glutamine by the enzyme glutamine synthetase (GS) in the human brain. We were able to acquire full datasets comprising two $[^{13}\text{N}]$ ammonia (test and retest) scans, two $[^{15}\text{O}]$ water scans and corresponding arterial input functions in five subjects, each on a single day.

Table 3 Repeatability metrics for [¹³N]ammonia one-tissue compartment (reversible) model parameters for grey matter and selected regions of interest (ROIs)

ROI	K_1 [$n=5$] (mL/100 g/min)					k_2 [$n=5$] (1/min)				
	S1	S2	ICC	VAR	AbsVAR	S1	S2	ICC	VAR	AbsVAR
Grey Matter	20.1 ± 1.5	18.6 ± 1.3	-0.83	-8 ± 14	10 ± 12	0.0069 ± 0.0029	0.0074 ± 0.0022	0.58	11 ± 38	28 ± 24
White matter	14.5 ± 1.2	13.5 ± 0.8	-0.89	-7 ± 14	9 ± 11	0.0059 ± 0.0027	0.0064 ± 0.0021	0.57	12 ± 43	32 ± 27
Hippocampus_l	18.9 ± 2.4	17.6 ± 1.0	-0.06	-7 ± 14	10 ± 11	0.0122 ± 0.0061	0.0144 ± 0.0041	0.89	23 ± 27	25 ± 24
OL_ling_G_l	23.7 ± 3.0	21.5 ± 1.0	-0.41	-9 ± 15	10 ± 14	0.0072 ± 0.0023	0.0075 ± 0.0020	0.58	5 ± 30	24 ± 15
G_cing_post_l	22.2 ± 1.6	20.6 ± 1.3	-0.68	-7 ± 13	9 ± 11	0.0065 ± 0.0032	0.0075 ± 0.0019	0.58	19 ± 40	30 ± 31
Putamen_l	23.3 ± 1.9	21.1 ± 1.5	-0.83	-10 ± 15	12 ± 12	0.0063 ± 0.0028	0.0072 ± 0.0028	0.59	13 ± 44	34 ± 27
Thalamus_l	22.5 ± 2.1	20.7 ± 1.1	-0.79	-8 ± 15	10 ± 13	0.0089 ± 0.0030	0.0101 ± 0.0024	0.72	15 ± 23	24 ± 9
Cerebellum_l	22.4 ± 2.0	20.6 ± 1.3	-0.69	-8 ± 14	9 ± 13	0.0061 ± 0.0027	0.0072 ± 0.0022	0.61	19 ± 39	33 ± 25

The table presents the intraclass correlation coefficient (ICC), percent mean fractional difference (VAR) and percent absolute fractional difference (AbsVAR) across test (S1) and retest (S2) scans. Data are presented as mean ± standard deviation for grey matter, white matter and the left (l) hippocampus, lingual gyrus (OL_ling_G), posterior cingulate gyrus (G_cing_post), putamen, thalamus, and cerebellum



Kinetic modelling in these subjects was unable to reliably estimate the rate constant relating to GS activity (k_3) from that related to [¹³N]ammonia brain uptake (K_1) and indicated non-negligible back-flux of [¹³N] from the brain to the blood. In addition, comparison of K_1 estimates with [¹⁵O]water CBF across brain regions and within-subjects found that these measures were highly correlated and of comparable reliability. Together these results indicate that the applied [¹³N]ammonia PET method is unable to quantify GS activity in the human brain, and instead may principally index CBF.

Studies in experimental animals have indicated [¹³N] ammonia PET might be able to index GS activity, as irreversible blockade of GS with methionine sulfoximine (MSO) decreases the brain [¹³N]ammonia signal [34]. In kinetic modelling of dynamic [¹³N]ammonia PET images of the human brain, GS activity would be captured by the rate constant k_3 in an irreversible two tissue compartment model. Using this model, our analysis returned values for k_3 that were highly variable within subjects, as well as between subjects and across grey matter regions. In most instances, k_3 values were also too low

to be estimated compared to the estimated error. Only one region of 79, left hippocampus, favoured a model including a k_3 parameter in a majority of subjects, however, considering the small number (3/5) and the poor estimability of k_3 in this region it is possible this is a false positive, though we present the data for future interest. A previous [^{13}N]ammonia study in subjects with cirrhosis and healthy volunteers using similar methodology was also unable to provide estimates of k_3 [20]. While volume of distribution ($V_T = K_1/k_2$) may potentially have provided a surrogate index of GS activity from a reversible model, we were also unable to reliably estimate k_2 , with absolute variability of both k_2 and V_T around 30% (Additional file 1: Table S11). Overall, this indicates that [^{13}N]ammonia PET is unlikely to be a suitable method for measuring the rate of metabolism of glutamate to glutamine by GS in the human brain.

Although the question as to whether ammonia in the brain can diffuse into the blood has previously been debated [35], back-flux of [^{13}N]ammonia from brain to blood has now been demonstrated in healthy volunteers as well as subjects with cirrhosis [11, 19, 20]. Similar to these studies, our finding of small but positive values for [^{13}N]ammonia k_2 also indicate nonzero back-flux of ^{13}N to blood. Consistent with this, the simplest irreversible model with a single tissue compartment and one rate constant, K_1 , showed a poor fit in nearly every dataset. The presence of non-negligible wash-out was also consistent with the plateau of the decay-corrected brain time-activity curves in conjunction with approximately 10% of parent tracer compound remaining in the arterial plasma at the end of the scan. Patlak plots were nonlinear at late times, also indicating the presence of reversibility of the tracer. Our data as well as that of Goldbecker et al. [20] indicate that back-flux of ammonia may be observed (although not reliably quantified) within 30 min of [^{13}N]ammonia injection. Potential biochemical explanations for washout could include the immediate back-flux of ammonia as well as a longer-term action of glutaminase recycling ^{13}N from the neuron back to the astrocyte [36].

The candidate compartmental models considered for [^{13}N]ammonia in this study assumed that no ^{13}N labelled metabolites crossed the blood brain barrier and contributed to brain tissue signal. We did not test this assumption explicitly, however, metabolites entering the brain would require a more complex kinetic model and would likely make the estimation of k_3 in the parent [^{13}N]ammonia component even less reliable due to increased numbers of parameters.

The process used in this study to separate parent [^{13}N]ammonia from ^{13}N labelled metabolites was taken from the method described by Keiding et al. [11]. However, over- or underestimated parent fractions from any

uncertainties in this method and fitted model would affect the parent plasma input function and therefore the kinetic analysis. The model comparisons favoured a one-tissue compartment. If the parent fraction model overestimated the true plasma [^{13}N]ammonia concentration, a positive k_2 could be a bias to fit the data better and k_3 even less likely separable from K_1 . An underestimate of parent plasma fraction would likely consider k_2 an underestimate of true washout, though again is unlikely to improve k_3 estimates.

Although k_2 ICC values were high in this study, the parameter estimates correspond to a half-life of approximately 100 min and accurate parameter estimates would typically require longer scan durations and consequently isotopes with more suitable half-lives. Though dependent on noise levels and simulated model specifics, Turkheimer et al. [39] found the slowest identifiable components close to those corresponding to scan duration. Therefore we would not consider these values to be truly representative without further work.

While our data did not support estimation of GS activity, it did indicate that [^{13}N]ammonia PET may provide an index of CBF. [^{13}N]ammonia K_1 correlated with the K_1 (CBF) from the preceding [^{15}O]water scans in the same subjects, and based on fractional difference metrics, [^{13}N]ammonia brain uptake (K_1) was of comparable reproducibility to [^{15}O]water CBF measures over the test and retest scanning sessions. The correlations between K_1 and CBF were observed when K_1 was calculated with either a reversible one-tissue or reversible two-tissue compartment model, and to a lesser extent between K_i (calculated using Patlak analysis) and CBF. The correlations between K_1 and CBF were qualitatively tighter for K_1 calculated from the one compared to two-tissue compartmental model, as would be expected given there are fewer parameters. Nonetheless the slope of the best fit was not identical between subjects and scans (Fig. 3). Correlating CBF and K_1 within region, across subjects and scans, did not yield significant correlations. In rhesus monkeys, Phelps et al. [37] found nonlinear relationships between K_1 (or specifically extraction fraction, EF) and CBF, over a wide range of CBF values. Our data indicate that a linear relationship between K_1 and CBF exists when CBF lies within the normal range investigated here.

Compared to the previous study of Keiding et al. [11] the values for [^{13}N]ammonia K_1 obtained in our study are approximately 35% lower and approximately 20% lower for CBF, though relative K_1 and CBF between basal ganglia (putamen and thalamus), cerebellum and cortex were similar. In addition, inter-subject variances of both parameters were comparable to that study. The absolute values of CBF were also in keeping with the variances seen between centres for quantitative PET studies

(approximately 40–60 mL/min 100g), as well as inter-scan and inter-subject variability (approximately 10%) [38]. The estimates for permeability-surface area product values and Flux_{met} were similar, while PS_{met} estimates were also slightly lower in our study, which is consistent with lower K_{met} found from the possibly unsuitable graphical method. As in Keiding et al., [11] we applied the Patlak method [32] to calculating K_{met} which avoided replicating the poor identification of k_2 and k_3 values with an explicit calculation. Nonetheless the fractional differences for K_{met} , PS_{met} and Flux_{met} between test and retest scans were high.

This work uses standard PET acquisition and analysis methodology, however the rapid incorporation of ammonia into glutamine [29] along with the practicalities of using short half-life tracers (2.03 min and 9.97 min for ^{15}O and ^{13}N , respectively) and multiple scans with blood sampling within one day present challenges to accurately measuring the tracer kinetics which could have impacted parameter identifiability, model selection and repeatability. A number are explored here in more detail.

Measured blood curves would be delayed and dispersed between the arterial sampling point and the PET signal (further exaggerated by the length of the line from the arterial cannula to the Allogg detector). CBF was calculated with delay and dispersion explicitly included in the model fits [27], though standard 1TCM and 2TCM were explored for ^{13}N ammonia kinetics without this accounted for. As noted in work by Toussaint and Meyer [40] delay and dispersion estimates can be highly correlated, so while including these parameters improves accuracy of CBF, their individual estimates can be inaccurate. We did extend the 5-parameter Meyer model for CBF up to a 7-parameter 2TCM (i.e. including k_3 , k_4 , delay and dispersion) and applied this to the ^{13}N ammonia data analysis, however this did not improve k_3 estimates and the preferred model remained the reversible 1TCM. In addition, increasing the number of free parameters increased the correlation and errors in parameter estimates.

Despite the preliminary work from simulations and dry runs, due to the blood processing time and to avoid low counts from ^{13}N decay in subsequent scans, blood sample timings for ^{13}N ammonia scans were changed after the first subject's scans (see Fig. 1, blue circles and lines) from 5-min intervals to those described in the methods. However the parent fraction fit is well within those of the remaining subjects used for the main analysis and those found by Keiding et al. [11] so we believe it is reasonable to assume this impact would be negligible.

Two errors in acquisition for some scans could have impacted the repeatability in CBF and/or K_1 . Subjects 1 and 2 did not have manual blood samples measured

for the ^{15}O water scans. For these subjects, the average plasma-over-blood values from all remaining subjects were used (mean 1.14, s.d. 0.03). For the 2nd pair of scans for subject 3 and all 4 scans for subject 4, equipment failure meant that the exact timing of the continuous blood sampler was not recorded directly but was estimated from unsynced system logs after assessment of complete datasets. As an example, for ^{15}O , a 20 s delay would result in a 12% bias from incorrect decay correction (2% for ^{13}N). Both these errors (plasma and sampler timing) would effect the scaling of the plasma input functions but not other properties, hence there may be biases in CBF and K_1 for these subjects, but not other rate-constants or model selection.

The parent fraction model was taken from the work of Keiding et al. [11], however the earliest blood sample was taken 4 min after tracer injection by which point most subjects showed a parent fraction under 50% (Fig. 1). It is possible that the biexponential fit is not ideal at earlier times and could influence the shape of the parent plasma curve, which may be necessary to accurately capture rapid kinetics. Similarly rapidly changing plasma-over-blood ratios (Additional file 1: Figure S2) would also have a similar impact. However, with standard PET methodology, continuous arterial sampling, while providing a detailed trace of the arterial concentration, does limit the ability to acquire large enough manual samples for further analysis without impacting the measurement of the blood peak.

The parent fraction estimation was also complicated by the outlying data from subjects 6, 7 and 8 (Fig. 1: black symbols and lines) in terms of values comparative to the remaining subjects or Keiding's [11] data quality as well a quality of fit to the biexponential model. Smaller sample size does not just limit power but may also increase the impact of outliers. For the main analysis we considered data from the first 5 subjects only, however the analysis from all subjects did not improve repeatability (Additional file 1: Tables S8 and S9) or model selection. A population parent fraction curve from the first 5 subjects was also used to for model fits but neither did this improve repeatability or model selection for 2TCM.

Repeatability may have been limited by participant fatigue during the second scanning session, due to the technical complexity of the study and as subjects remained in the PET centre for an average of 3.5 h between the start of the first scan and end of the last. However, interscan variability for CBF and K_1 were comparable and in line with previous CBF studies [38].

The strong correlations observed between K_1 and CBF yielded variable slopes between subjects and scan pairs. It is unclear how much is attributable to a true

representation of physiology or to unforeseen errors from the challenges of complex timing with short half-life tracers.

While the CBF and K_1 ($[^{13}\text{N}]$ ammonia) correlated well within each scan pair, this study did not investigate the quantification or detectability of changes in perfusion per se. However, PET tracers with longer radioisotope half-lives are in general easier to incorporate into a scanning schedule and the slower washout of $[^{13}\text{N}]$ ammonia may yield images with improved signal to noise compared to $[^{15}\text{O}]$ water. Our results therefore suggest that the use of $[^{13}\text{N}]$ ammonia as a brain perfusion marker for low to normal blood flow may warrant further investigation.

Conclusions

Based on our data, cerebral glutamate synthetase activity is not quantifiable using $[^{13}\text{N}]$ ammonia PET in healthy volunteers. Over a 30-min uptake period, tissue wash-out of the tracer is identifiable with a simple one-tissue compartmental model, suggesting irreversible models are not strictly appropriate. While the most repeatable uptake parameter, K_1 , would likely be a macroparameter combining perfusion, PS product and GS activity rather than assessing GS activity per se, it appears to correlate well with CBF and may be useful in this context.

Supplementary information

Supplementary information accompanies this paper at <https://doi.org/10.1186/s13550-020-00731-0>.

Additional file 1. Supplementary Information.

Acknowledgements

None.

Authors' contributions

AE and AG conceptualised and designed the study. The study protocol was developed together with methodological input from JTD, NS, ZY, JO'D, AH, FET and PKM. ZY, JO'D, NS and AG optimised and performed the radiosynthesis and radiometabolite assays and analyses. JTD conducted neuroimaging analyses. ZY and JTD conducted metabolite analyses. NS, AE and IK recruited and screened study participants. IK, JM, and SC were study clinicians. AE, JTD, NS, ZY, FET, PKM, AH and AG interpreted study data. Preparation of the manuscript was led by AE, JTD and NS with contributions from all authors. All authors read and approved the final manuscript.

Funding

This work was supported by the Wellcome/EPSCRC Centre for Medical Engineering (WT 203148/Z/16/Z) and by the National Institute for Health Research (NIHR) Biomedical Research Centre at South London and Maudsley NHS Foundation Trust and King's College London. The views expressed are those of the authors and not necessarily those of the NHS, the NIHR or the Department of Health and Social Care.

Availability of data and materials

The datasets used during the current study are available from the corresponding author on reasonable request.

Ethics approval and consent to participate

The study had ethical approval from the NHS Ethical Committee (NRES South East Coast, Surrey, Ref: 13/LO/0146), the local Research and Development offices and the Administration of Radioactive Substances Advisory Committee (ARSAC, Certificate RPC 261/3186/29926). All procedures were performed in accordance with the ethical standards of the research committee and with the 1964 Helsinki Declaration and its later amendments. Informed consent was obtained from all individual participants included in the study.

Consent for publication

Not applicable.

Competing interests

The authors declare that they have no competing interests.

Author details

¹ Department of Psychosis Studies, Institute of Psychiatry, Psychology and Neuroscience, King's College London, 16 De Crespigny Park, London SE5 8AF, UK. ² School of Biomedical Engineering and Imaging Sciences, St Thomas' Hospital, King's College London, London SE1 7EH, UK. ³ King's College London & Guy's and St. Thomas' PET Centre, London SE1 7EH, UK. ⁴ Department of Neuroimaging, Institute of Psychiatry, Psychology and Neuroscience, King's College London, London SE5 7AF, UK. ⁵ Present Address: Department of Psychiatry, Warneford Hospital, University of Oxford, Oxford OX3 7JX, UK. ⁶ Present Address: Clinical Imaging Research Centre, National University of Singapore, Singapore 117599, Singapore.

Received: 19 May 2020 Accepted: 21 November 2020

Published online: 03 December 2020

References

- Martinez-Hernandez A, Bell KP, Norenberg MD. Glutamine synthetase: glial localization in brain. *Science*. 1977;195(4284):1356–8. <https://doi.org/10.1126/science.14400>.
- Eid T, Gruenbaum SE, Dhaher R, Lee TW, Zhou Y, Danbolt NC. The glutamate–glutamine cycle in epilepsy. *Adv Neurobiol*. 2016;13:351–400. https://doi.org/10.1007/978-3-319-45096-4_14.
- Rose CF, Verkhratsky A, Parpura V. Astrocyte glutamine synthetase: pivotal in health and disease. *Biochem Soc Trans*. 2013;41(6):1518–24. <https://doi.org/10.1042/BST20130237>.
- Eid T, Lee TW, Patrylo P, Zaveri HP. Astrocytes and glutamine synthetase in epileptogenesis. *J Neurosci Res*. 2019;97(11):1345–62. <https://doi.org/10.1002/jnr.24267>.
- Haberle J, Gorg B, Toutain A, Rutsch F, Benoist JF, Gelot A, et al. Inborn error of amino acid synthesis: human glutamine synthetase deficiency. *J Inher Metab Dis*. 2006;29(2–3):352–8. <https://doi.org/10.1007/s10545-006-0256-5>.
- Spodenkiewicz M, Diez-Fernandez C, Rufenacht V, Gemperle-Britschgi C, Haberle J. Minireview on glutamine synthetase deficiency, an ultra-rare inborn error of amino acid biosynthesis. *Biology (Basel)*. 2016. <https://doi.org/10.3390/biology5040040>.
- Zhou Y, Dhaher R, Parent M, Hu QX, Hassel B, Yee SP, et al. Selective deletion of glutamine synthetase in the mouse cerebral cortex induces glial dysfunction and vascular impairment that precede epilepsy and neurodegeneration. *Neurochem Int*. 2019;123:22–33. <https://doi.org/10.1016/j.neuint.2018.07.009>.
- Eid T, Thomas MJ, Spencer DD, Runden-Pran E, Lai JC, Malthankar GV, et al. Loss of glutamine synthetase in the human epileptogenic hippocampus: possible mechanism for raised extracellular glutamate in mesial temporal lobe epilepsy. *Lancet*. 2004;363(9402):28–37. [https://doi.org/10.1016/S0140-6736\(03\)15166-5](https://doi.org/10.1016/S0140-6736(03)15166-5).
- van der Hel WS, Notenboom RG, Bos IW, van Rijen PC, van Veelen CW, de Graan PN. Reduced glutamine synthetase in hippocampal areas with neuron loss in temporal lobe epilepsy. *Neurology*. 2005;64(2):326–33. <https://doi.org/10.1212/01.WNL.0000149636.44660.99>.
- Benjamin AM, Quastel JH. Metabolism of amino acids and ammonia in rat brain cortex slices in vitro: a possible role of ammonia

- in brain function. *J Neurochem*. 1975;25(3):197–206. <https://doi.org/10.1111/j.1471-4159.1975.tb06953.x>.
11. Keiding S, Sorensen M, Bender D, Munk OL, Ott P, Vilstrup H. Brain metabolism of ^{13}N -ammonia during acute hepatic encephalopathy in cirrhosis measured by positron emission tomography. *Hepatology*. 2006;43(1):42–50. <https://doi.org/10.1002/hep.21001>.
 12. Lockwood AH, Bolomey L, Napoleon F. Blood-brain barrier to ammonia in humans. *J Cereb Blood Flow Metab*. 1984;4(4):516–22. <https://doi.org/10.1038/jcbfm.1984.76>.
 13. Lockwood AH, McDonald JM, Reiman RE, Gelbard AS, Laughlin JS, Duffy TE, et al. The dynamics of ammonia metabolism in man. Effects of liver disease and hyperammonemia. *J Clin Invest*. 1979;63(3):449–60. <https://doi.org/10.1172/JCI109322>.
 14. Lockwood AH, Yap EW, Wong WH. Cerebral ammonia metabolism in patients with severe liver disease and minimal hepatic encephalopathy. *J Cereb Blood Flow Metab*. 1991;11(2):337–41. <https://doi.org/10.1038/jcbfm.1991.67>.
 15. Ahl B, Weissenborn K, van den Hoff J, Fischer-Wasels D, Kostler H, Hecker H, et al. Regional differences in cerebral blood flow and cerebral ammonia metabolism in patients with cirrhosis. *Hepatology*. 2004;40(1):73–9. <https://doi.org/10.1002/hep.20290>.
 16. Weissenborn K, Bokemeyer M, Ahl B, Fischer-Wasels D, Giewekemeyer K, van den Hoff J, et al. Functional imaging of the brain in patients with liver cirrhosis. *Metab Brain Dis*. 2004;19(3–4):269–80.
 17. Keiding S, Sorensen M, Munk OL, Bender D. Human (13)N-ammonia PET studies: the importance of measuring (13)N-ammonia metabolites in blood. *Metab Brain Dis*. 2010;25(1):49–56. <https://doi.org/10.1007/s11011-010-9181-2>.
 18. Sorensen M, Keiding S. New findings on cerebral ammonia uptake in HE using functional (13)N-ammonia PET. *Metab Brain Dis*. 2007;22(3–4):277–84. <https://doi.org/10.1007/s11011-007-9066-1>.
 19. Sorensen M, Munk OL, Keiding S. Backflux of ammonia from brain to blood in human subjects with and without hepatic encephalopathy. *Metab Brain Dis*. 2009;24(1):237–42. <https://doi.org/10.1007/s11011-008-9126-1>.
 20. Goldbecker A, Buchert R, Berding G, Bokemeyer M, Lichtiginghagen R, Wilke F, et al. Blood-brain barrier permeability for ammonia in patients with different grades of liver fibrosis is not different from healthy controls. *J Cereb Blood Flow Metab*. 2010;30(7):1384–93. <https://doi.org/10.1038/jcbfm.2010.22>.
 21. He Q, Zhang L, Zhang B, Shi X, Yi C, Zhang X. Diagnostic accuracy of (13)N-ammonia PET, (11)C-methionine PET and (18)F-fluorodeoxyglucose PET: a comparative study in patients with suspected cerebral glioma. *BMC Cancer*. 2019;19(1):332. <https://doi.org/10.1186/s12885-019-5560-1>.
 22. Wieland B, Bida G, Padgett H, Hendry G, Zippi E, Kabalka G, et al. In-target production of [N-13] ammonia via proton irradiation of dilute aqueous ethanol and acetic-acid mixtures. *Appl Radiat Isotopes*. 1991;42(11):1095–8.
 23. Berridge MS, Terris AH, Cassidy EH. Low-carrier production of [O-15] oxygen water and carbon-monoxide. *Appl Radiat Isotopes*. 1990;41(12):1173–5.
 24. Gousias IS, Rueckert D, Heckemann RA, Dyet LE, Boardman JP, Edwards AD, et al. Automatic segmentation of brain MRIs of 2-year-olds into 83 regions of interest. *Neuroimage*. 2008;40(2):672–84. <https://doi.org/10.1016/j.neuroimage.2007.11.034>.
 25. Hammers A, Allom R, Koepp MJ, Free SL, Myers R, Lemieux L, et al. Three-dimensional maximum probability atlas of the human brain, with particular reference to the temporal lobe. *Hum Brain Mapp*. 2003;19(4):224–47. <https://doi.org/10.1002/hbm.10123>.
 26. Ashburner J, Friston KJ. Unified segmentation. *Neuroimage*. 2005;26(3):839–51. <https://doi.org/10.1016/j.neuroimage.2005.02.018>.
 27. Meyer E. Simultaneous correction for tracer arrival delay and dispersion in CBF measurements by the H215O autoradiographic method and dynamic PET. *J Nucl Med*. 1989;30(6):1069–78.
 28. DeGrado TR, Hanson MW, Turkington TG, DeLong DM, Brezinski DA, Vallee JP, et al. Estimation of myocardial blood flow for longitudinal studies with ^{13}N -labeled ammonia and positron emission tomography. *J Nucl Cardiol*. 1996;3(6 Pt 1):494–507.
 29. Cooper AJ, McDonald JM, Gelbard AS, Gledhill RF, Duffy TE. The metabolic fate of ^{13}N -labeled ammonia in rat brain. *J Biol Chem*. 1979;254(12):4982–92.
 30. Veronese M, Rizzo G, Bertoldo A, Turkheimer FE. Spectral analysis of dynamic PET studies: a review of 20 years of method developments and applications. *Comput Math Methods Med*. 2016;2016:7187541. <https://doi.org/10.1155/2016/7187541>.
 31. Akaike H. Likelihood of a model and information criteria. *J Econom*. 1981;16(1):3–14. [https://doi.org/10.1016/0304-4076\(81\)90071-3](https://doi.org/10.1016/0304-4076(81)90071-3).
 32. Patlak CS, Blasberg RG, Fenstermacher JD. Graphical evaluation of blood-to-brain transfer constants from multiple-time uptake data. *J Cereb Blood Flow Metab*. 1983;3(1):1–7. <https://doi.org/10.1038/jcbfm.1983.1>.
 33. McGraw KO, Wong SP. Forming inferences about some intraclass correlation coefficients. *Psychol Methods*. 1996;1(1):30–46. <https://doi.org/10.1037/1082-989x.1.1.30>.
 34. Momosaki S, Ito M, Tonomura M, Abe K. Assessment of glutamine synthetase activity by [13N]ammonia uptake in living rat brain. *Synapse*. 2015;69(1):26–32. <https://doi.org/10.1002/syn.21781>.
 35. Ott P, Larsen FS. Blood-brain barrier permeability to ammonia in liver failure: a critical reappraisal. *Neurochem Int*. 2004;44(4):185–98.
 36. Cooper AJ. ^{13}N as a tracer for studying glutamate metabolism. *Neurochem Int*. 2011;59(4):456–64. <https://doi.org/10.1016/j.neuint.2010.11.011>.
 37. Phelps ME, Huang SC, Hoffman EJ, Selin C, Kuhl DE. Cerebral extraction of N-13 ammonia: its dependence on cerebral blood flow and capillary permeability—surface area product. *Stroke*. 1981;12(5):607–19. <https://doi.org/10.1161/01.str.12.5.607>.
 38. Fan AP, Jahanian H, Holdsworth SJ, Zaharchuk G. Comparison of cerebral blood flow measurement with [15O]-water positron emission tomography and arterial spin labeling magnetic resonance imaging: a systematic review. *J Cereb Blood Flow Metab*. 2016;36(5):842–61. <https://doi.org/10.1177/0271678X16636393>.
 39. Turkheimer F, Moresco RM, Lucignani G, Sokoloff L, Fazio F, Schmidt K. The use of spectral analysis to determine regional cerebral glucose utilization with positron emission tomography and [^{18}F]fluorodeoxyglucose: theory, implementation, and optimization procedures. *J Cereb Blood Flow Metab*. 1994;14(3):406–22. <https://doi.org/10.1038/jcbfm.1994.52> (PMID: 8163583).
 40. Toussant PJ, Meyer E. A sensitivity analysis of model parameters in dynamic blood flow studies using H_2^{15}O and PET. In: Myers R, Cunningham V, Bailey D, Jones T, editors. Quantification of brain function using PET. London: Academic Press; 1996.

Publisher's Note

Springer Nature remains neutral with regard to jurisdictional claims in published maps and institutional affiliations.